Self-excitability of roller coaster trains along spatial trajectories

Marc G. Zamora Agustí, Andrés Kecskeméthy

Fakultät für Ingenieurwissenschaften
Universität Duisburg-Essen
Lotharstraße 1, 47057 Duisburg, Deutschland
[marc.zamora-agusti@stud.uni-due.de, andres.kecskemethy@uni-due.de]

ABSTRACT

It is well known that vibrations usually appear during a roller coaster ride, which in some cases leads to passenger discomfort and poses additional material and structural strain. However, the causes of such vibrations are still not fully understood. While there have been technological advances that help to mitigate them to some degree, for instance by placing shock absorbers between the wheels and the bogie frame, an analysis of this phenomenon is required to make better decisions at the design stage. For the first time to the knowledge of the authors, in this investigation the problem is analyzed from the point of view of a self-excited dynamical system, thus ruling out trajectory deviations or local defects. A mechanical model is proposed, consisting in the separation of the overall spatial trajectory motion from the relative motions between train components and the representation of the wrenches at the end bodies of the kinematical chain using a simplified bogie-rail contact approach. Furthermore, the contact problem is extended with respect to previous works by considering the creep forces in the contact interface. Regions of increased oscillations are observed, indicating a possible self-excitation in real systems.

Keywords: vibrations, roller coasters, self-excited oscillations.

1 INTRODUCTION

The simulation of roller coaster rides, often employing multibody dynamics formulations, is ubiquitous in the industry. During the layout design process, the track must be shaped and corrected based on different criteria, one of the most important being the passenger accelerations or g-loads. To this end, either simplistic models or complex multibody systems can be used. For example, a simple mass point moving along a spatial trajectory roughly yields the vehicle centripetal forces, whereas a more complete model regarding several rigid degrees of freedom can more accurately describe the individual passenger trajectories and even be used for collision analysis. The latter usually features a closed kinematical topology, which requires few parameters and can be solved notably fast. Nonetheless, this type of formulation can rarely capture the vibrational behavior of the real system.

A simple extension to a perfectly rigid formulation is the lumped mass approach, as proposed in [1] for a quarter-carbody model subject to trajectory deviations modeled as a stationary Gaussian process. In [2], a two-wheel car system regarding a lumped mass model of the passengers is also proposed. Also, a complete roller coaster train of rigid bodies with a compliant contact model was studied in [3], using real rail trajectory deviation data. Nonetheless, a mismatch between the simulated spatial frequencies and the measurements was observed. These results are the main motivation for the present study, based on the hypothesis that self-excitation mechanisms may exist in roller coaster systems.

Several self-excited systems have been extensively studied in the literature, such as the shimmy phenomenon [4-6] or the rocking motion of trailers [7-8]. A common method to determine the bifurcation parameters is to apply classical stability analysis to the linearized system, or the center manifold theory, provided that low-dimensional analytical dynamical models are available. In a

roller coaster, the equilibrium points and the steady-state behavior become meaningless, given the rapidly changing configuration of the train along the trajectory. In the light of this, the time response will be analyzed instead.

2 MECHANICAL SYSTEM

2.1 IDEAL SYSTEM

Let n be the number of cars of a roller coaster train, $\mathbf{r}_{\mathrm{CL}}(s) \in \mathbb{R}^3$, $\mathbf{r}_{\mathrm{LR}}(s) \in \mathbb{R}^3$ and $\mathbf{r}_{\mathrm{RR}}(s) \in \mathbb{R}^3$ the arc-length parametrized spatial curves describing the track centerline (CL), left rail (LR) and right rail (RR), and $\mathbf{R}(s) = [\hat{\mathbf{t}} \quad \hat{\mathbf{b}} \quad \hat{\mathbf{n}}] \in SO(3)$ their corresponding rotation matrices, which constitute a curve frame, so that $\mathrm{d}\mathbf{r}(s)/\mathrm{d}s = \hat{\mathbf{t}}(s)$. Also, let $\mathbf{q} \in \mathbb{R}^{f(n)}$ be the vector of generalized coordinates uniquely describing the configuration of the system, where $f(n)$ indicates a dependence on the number of wagons and the type of mechanism.

Various steering systems are currently used in roller coaster trains. Here, wheel bogies with independent kingpin will be considered (Figure 1), except for the front axle, rigidly attached to them. In Figure 1, $\boldsymbol{\varphi}_3$ represents an arbitrary rotation parametrization of the spherical joints with 3 coordinates, whereas $\boldsymbol{\varphi}_2$ corresponds to the yaw and pitch angles of the wheel bogies. Moreover, the front axle has 5 mobilities with respect to the centerline transform at s_z, 2 (y, z) corresponding to a movement on the plane with normal $\hat{\mathbf{t}}_{\mathrm{CL}}$ and 3 $(\boldsymbol{\varphi}_3)$ corresponding to an equivalent ball joint.

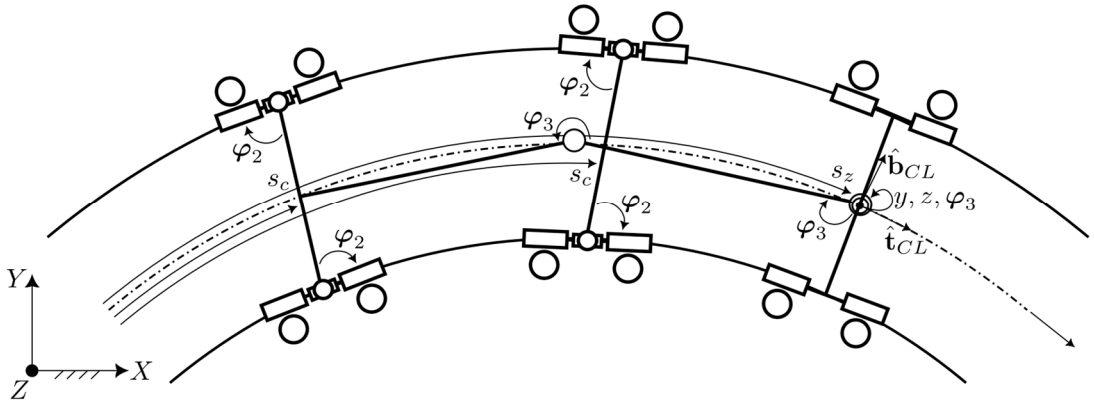

Figure 1. *Example of a roller coaster train mechanism with two cars and a front axle.*

The ideal system is described as the single degree of freedom mechanism uniquely determined by the centerline coordinate s_{z} that locates one reference body. In this case, the front axle is taken as reference, commonly termed zero-car. In view of this, the vector of generalized coordinates becomes $\mathbf{q} = [s_{\mathrm{z}} \quad \mathbf{q}_{\mathrm{d}}]$, where $\mathbf{q}_{\mathrm{d}} \in \mathbb{R}^{f(n)-1}$ is the vector of dependent generalized coordinates. Then, the dependent coordinates $\mathbf{q}_{\mathrm{d}}$ may be solved at fixed s_{z} steps, resulting in the mappings $q_{\mathrm{i}}^{(0)} = q_{\mathrm{i}}^{(0)}(s_{\mathrm{z}})$, for $i = 2, \ldots, f(n)$, where the superscript (0) refers to the ideal solution. In order to solve for $\mathbf{q}_{\mathrm{d}}$, a system of augmented constraint equations $\boldsymbol{\Phi}(\mathbf{q}_{\mathrm{d}}, \mathbf{s}_{\mathrm{c}}; s_{\mathrm{z}})$ is built, where $\mathbf{s}_{\mathrm{c}}$ is a vector of centerline coordinates and/or rail coordinates that refer to the bodies closing the kinematical chain. The constraint equations of the front axle are $y = z = 0$ and $\boldsymbol{\varphi}_3 = \mathbf{0}$. For an arbitrary car, the central point $\boldsymbol{p}_c$ between bogies is constrained along the centerline spline, so that $\boldsymbol{p}_{\mathrm{c}} = \mathbf{r}_{\mathrm{CL}}(s_{\mathrm{c}})$, and the roll angle is blocked, which can be expressed as $\hat{\mathbf{b}}_{\mathrm{CL}}^T(s_{\mathrm{c}})\hat{\mathbf{n}}_{\mathrm{c}} = 0$, where $\hat{\mathbf{n}}_{\mathrm{c}}$ is the normal vector of the car. In this kind of mechanism, the line between two bogies is not necessarily perpendicular to the rails. In order to take it into consideration, the centerline coordinate s_{c} may be corrected according to the relative angle between the car and centerline tangential directions $\hat{\mathbf{t}}_{\mathrm{c}}$ and $\hat{\mathbf{t}}_{\mathrm{CL}}$, getting s^*. Finally, the tangential direction of the bogies $\hat{\mathbf{t}}_{\mathrm{b}}$ is forced to guarantee $\hat{\mathbf{t}}_{\mathrm{b}}^T\hat{\mathbf{n}}_{\mathrm{CL}}(s^*) = 0$ and $\hat{\mathbf{t}}_{\mathrm{b}}^T\hat{\mathbf{b}}_{\mathrm{CL}}(s^*) = 0$. It is worth noting that the ideal system can be solved without the rail curves.

The precomputed ideal trajectories $q_{\mathrm{i}}^{(0)}(s_{\mathrm{z}})$ can be later used in the real system (Section 2.2) to initialize it at an arbitrary centerline location. Furthermore, the dynamics of the ideal system described here can be solved fast and will determine a reference centerline trajectory $s_{\mathrm{z}}(t)$. For

the vibration analysis of the real system, it will be convenient to compare the results for analogous positions and speeds along the track. For this purpose, the solution $s_{\mathrm{z}}(t)$ can be used to force a motion along the track, correcting the variation in dissipated energy between the different analyzed scenarios.

2.2 REAL SYSTEM

The real system consists of an open kinematical chain, described by the same generalized coordinates $\mathbf{q}$ as the ideal system, plus one additional coordinate per wheel, representing the rolling motion, and one additional rail coordinate per bogie.

The roller coaster train moves along the track due to the forces developing at each wheel-rail contact interface, for which the contact point must be calculated. Here, a simplified approach will be taken (Figure 2). The bogie rail coordinate s_b, referenced to a virtual bogie point between all 6 wheels, together with its relative orientation with respect to the rail tangent ($\hat{\mathbf{t}}_{\mathrm{b}}$ to $\hat{\mathbf{t}}_{\mathrm{R}}$), determines an approximate additional rail coordinate correction, locating a new rail coordinate for both the front (F) and rear (B) wheels of the same bogie, so that $s_{\mathrm{b}}^{(\mathrm{F})} = s_b + b\hat{\mathbf{t}}_{\mathrm{b}}^T\hat{\mathbf{t}}_{\mathrm{R}}$ and $s_{\mathrm{b}}^{(\mathrm{F})} = s_b - b\hat{\mathbf{t}}_{\mathrm{b}}^T\hat{\mathbf{t}}_{\mathrm{R}}$.

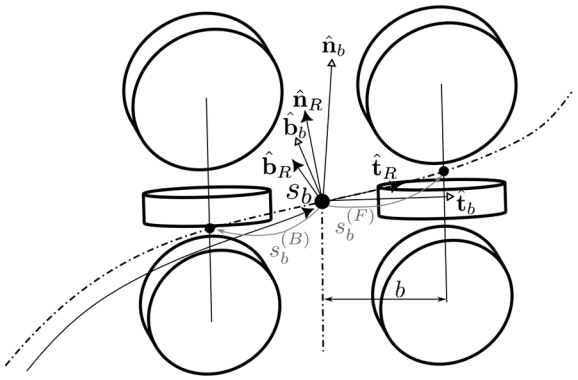

Figure 2. *Front and rear rail coordinates based on* s_{b}.

Once the rail coordinates are computed, a contact reference frame is determined to describe both the normal and tangential forces (Figure 3). The contact is assumed of the type cylinder-cylinder, and thus the normal direction is perpendicular to both of their axes (tangential direction of the rail $\hat{\mathbf{t}}_{\mathrm{R}}$ and rotating axis of the wheel $\hat{\mathbf{y}}_{\mathrm{w}}$), that is, $\hat{\mathbf{n}}_{\mathrm{k}} = (\hat{\mathbf{t}}_{\mathrm{R}} \times \hat{\mathbf{y}}_{\mathrm{w}})/\|\hat{\mathbf{t}}_{\mathrm{R}} \times \hat{\mathbf{y}}_{\mathrm{w}}\|$. Finally, the wheel heading direction is simply given by $\hat{\mathbf{h}} = \hat{\mathbf{y}}_{\mathrm{w}} \times \hat{\mathbf{n}}_{\mathrm{k}}$. The contact point velocity $\mathbf{v}_{\mathrm{k}}$ is decomposed into its heading and lateral components, respectively v_{h} and v_{s}, that are subsequently divided by the tangential speed $\|\mathrm{proj}_{\hat{\mathbf{n}}_{\mathrm{k}}}\{\mathbf{v}_{\mathrm{w}}\}\|$ to obtain the longitudinal and lateral creepages ξ_{x} and ξ_{y}. The same applies to the angular velocity component along $\hat{\mathbf{n}}_{\mathrm{k}}$, yielding the spin ξ_{ϕ}. The component of $\mathbf{v}_{\mathrm{w}}$ along $\hat{\mathbf{n}}_{\mathrm{k}}$ yields the penetration speed $\dot{\delta}$, whilst the penetration depth δ is the distance between the wheel rotation axis and the rail tangent minus their radii, respectively R_{w} and R_{R}.

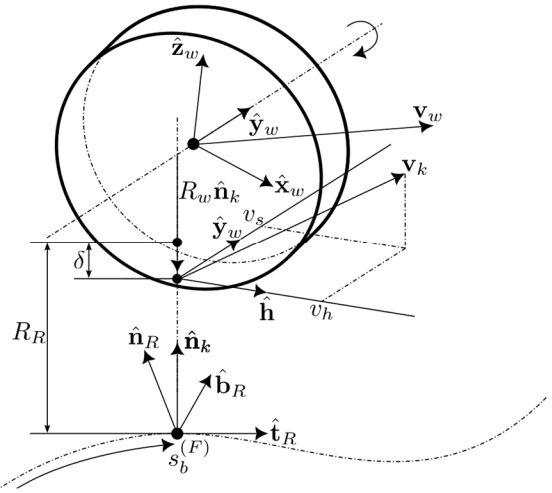

Figure 3. *Contact interface between a front running wheel and its respective rail axis.*

The contact response of the running wheels is mainly characterized by the direct contact of the PU thread with the rail. The following normal contact force model is assumed (see [9] for an extensive review), which takes into account the material damping occurring during a sustained contact for varying vertical g-loads:

$$\mathbf{F}_{\mathrm{N}} = \begin{cases} \left(k\delta^{n} + c\delta^{n-1}\dot{\delta}\right)\hat{\mathbf{n}}_{\mathrm{k}} & \delta > 0 \\ \mathbf{0} & \delta \leq 0 \end{cases}, \tag{1}$$

where $\mathbf{F}_{\mathrm{N}}$ is the normal force, k the stiffness coefficient and c the damping coefficient.

Conversely, the contact response of the lateral and upstop wheels is mainly determined by the shock absorber response. Given the lack of data on the viscoelastic behavior of these absorbers, the Kelvin-Voigt rheological model will be used:

$$\mathbf{F}_{\mathrm{N}} = \begin{cases} \left(k(\delta + \delta_0) + c\dot{\delta}\right)\hat{\mathbf{n}}_{\mathrm{k}} & \delta + \delta_0 > 0 \\ \mathbf{0} & \delta + \delta_0 \leq 0 \end{cases}, \tag{2}$$

where δ_0 is the initial compression of the viscoelastic absorber.

Also, the creep forces are determined by means of Polach's method [10], approximating the contact ellipse semiaxes in the heading and lateral directions. A rolling resistance torque is additionally applied by offsetting the normal force $\mathbf{F}_{\mathrm{N}}$ along the heading direction $\hat{\mathbf{h}}$.

2.3 EXCITATION SCENARIOS

In order to assess the vibrational behavior of the presented system, the following excitation scenarios can be considered:

a) The train moves along the designed trajectory without any additional excitation. That corresponds to a *soft excitation*, and it is the case regarded in this paper. The rapid but smooth trajectory changes act as the main perturbation.

b) The train moves along the designed trajectory, but it is perturbed at specified positions, either with impulses or bounded variations of the generalized coordinates. That could correspond to a *hard excitation*. After the perturbation, the train continues its movement along the designed track. Self-excited oscillations that are not observed in a) may arise and persist after a transient period.

c) The train moves along a perturbed trajectory, that is, with additional trajectory deviations and local defects. This is the case of an *external excitation*. A coupling between self-excited mechanisms and the forced perturbations may take place.

Scenarios b) and c) are a subject of future research. In Section 3, the results of two simulations corresponding to case a) are presented.

3 RESULTS

The mechanical system of the roller coaster train described in Section 2 is simulated along a fictive track with a prescribed centerline motion $s_{\mathrm{z}}(t)$. The track has been designed such that the chassis g-loads and speeds could be those of a real ride. Two different situations have been tested: without and with tangential contact forces. The g-loads of the chassis CM have been filtered with a high-pass filter to eliminate the low-frequency components corresponding to the ideal movement along a curve. Figure 4 shows the maximum value of the power spectral density (PSD) results per time, and Figure 5 per frequency. It can be observed that the tangential contact forces excite the system at some regions, thus indicating a possible self-excitation mechanism in real systems. Furthermore, the distinct responses among cars and with respect to time manifest the fact that both a complete train and a spatial trajectory must be taken into account when studying the vibrational response of a roller coaster. The peak at $t = 0$ in Figure 4 represents the fact that the system is initialized at an ideal configuration, as explained in Section 2.1, where the contact forces do not compensate the weight.

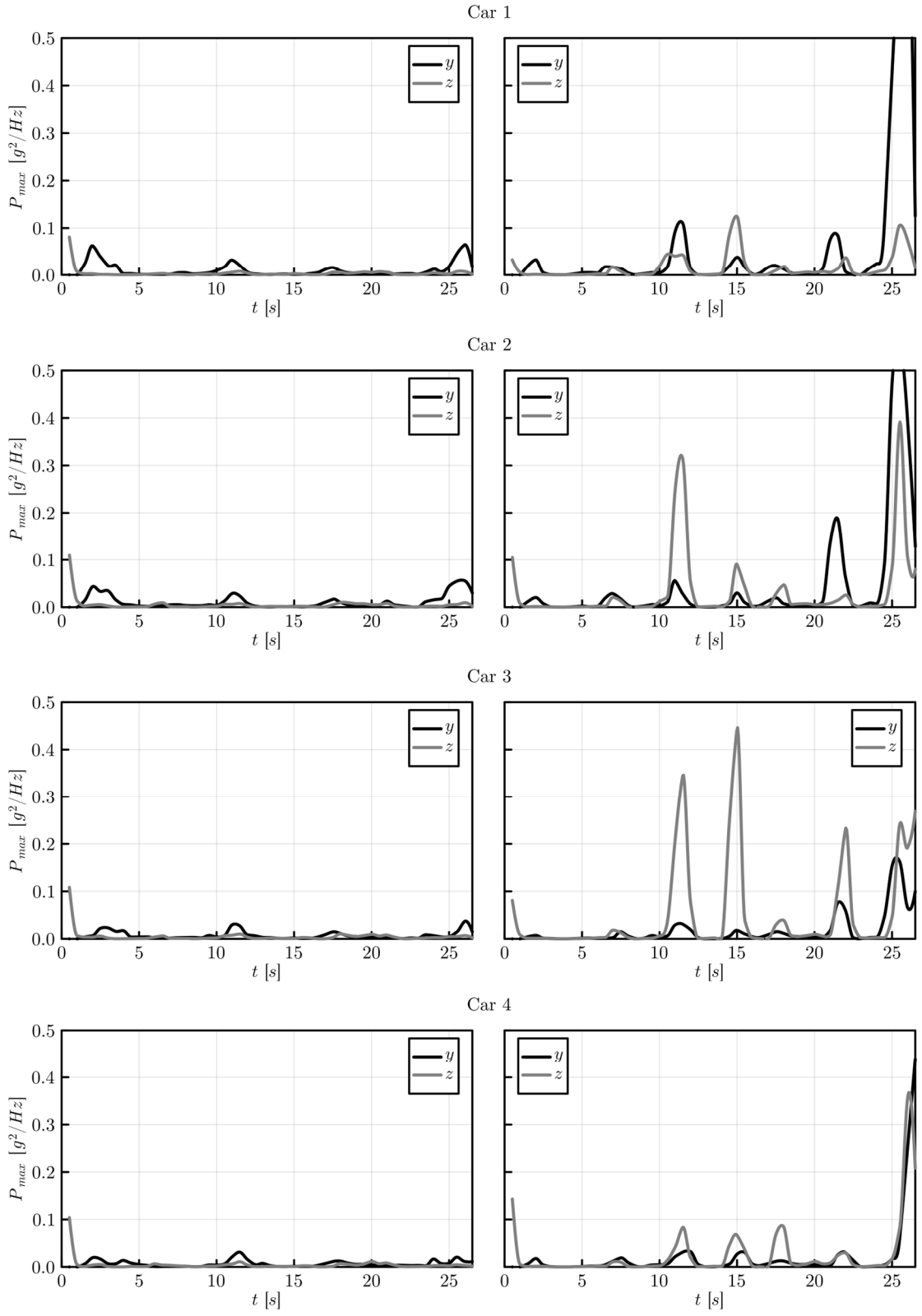

Figure 4. *Maximum PSD vs. time in lateral (y) and vertical (z) directions. Case without (left) and with (right) contact friction.*

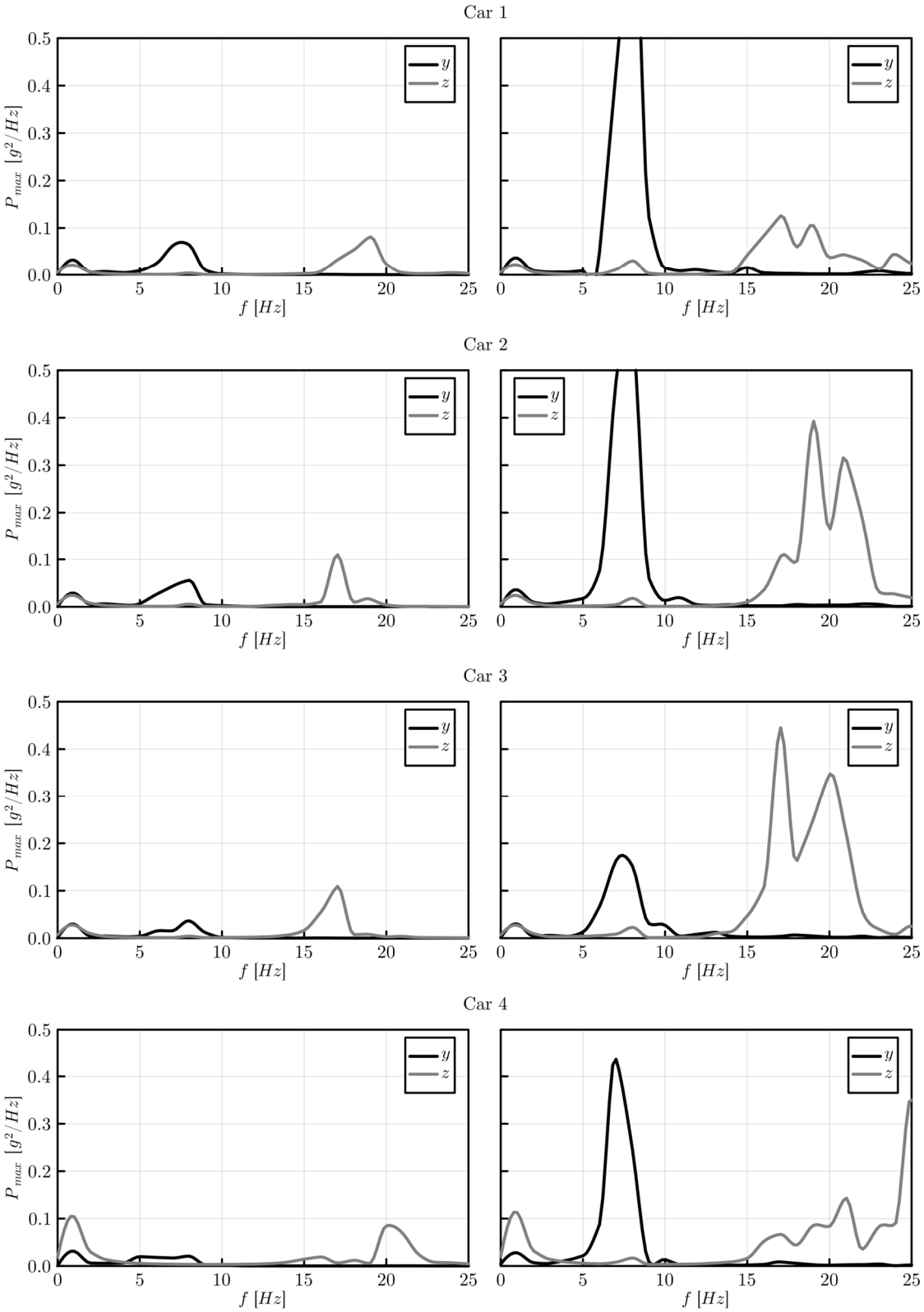

***Figure 5**. Maximum PSD vs. frequency in lateral (y) and vertical (z) directions. Case without (left) and with (right) contact friction.*

4 CONCLUSIONS

A mechanical model of a roller coaster train moving along spatial trajectories has been proposed, which takes into account the complete kinematics of a real steering mechanism and allows for a simple determination of the forces at each wheel-rail contact interface, with the novelty that the creep forces are also taken into account. It has been shown that without any additional perturbation, regions of increased oscillations arise at some track locations. The next step is to consider local hard excitations, to prove whether additional sustained self-excited regimes may emerge.

REFERENCES

[1] Zheng, L. H., Z. Liu, M. L. Chen, and Y. T. Zhu. 'Vibration Modeling and Position-Dependent Analysis of Spatial Trajectory Roller Coaster'. *Archive of Applied Mechanics* 87, no. 3 (March 2017): 489–502. https://doi.org/10.1007/s00419-016-1206-9.

[2] Fujita, Katsuhisa, Koichi Katsuoka, and Hiroaki Toshimitsu. 'Dynamics of Two-Wheels Modeling Roller Coaster Running on a Complicated 3 Dimensional (3D) Trajectory Considering Air Resistance'. *Journal of System Design and Dynamics* 5, no. 3 (2011): 403–15. https://doi.org/10.1299/jsdd.5.403.

[3] Malessa, Christian Sebastian. 'Eine objektorientierte Simulationsumgebung für die Analyse von Schwingungsvorgängen bei Achterbahnfahrten'. PhD, Universität Duisburg-Essen, 2016.

[4] Stépán, G. 'Chaotic Motion of Wheels'. *Vehicle System Dynamics* 20, no. 6 (January 1991): 341–51. https://doi.org/10.1080/00423119108968994.

[5] Brearley, M. N. 'Investigation of Castor-Wheel Shimmy'. *The Quarterly Journal of Mechanics and Applied Mathematics* 33, no. 4 (1980): 491–505. https://doi.org/10.1093/qjmam/33.4.491.

[6] Lu, Jianwei, Yi Xu, Chen Hu, Alexander F. Vakakis, and Lawrence A. Bergman. '5-DOF Dynamic Model of Vehicle Shimmy System with Clearance at Universal Joint in Steering Handling Mechanism'. *Shock and Vibration* 20, no. 5 (2013): 951–61. https://doi.org/10.1155/2013/469497.

[7] Horvath, Zoltan, and Denes Takacs. 'Analogue Models of Rocking Suitcases and Snaking Trailers'. In *Nonlinear Dynamics of Structures, Systems and Devices*, edited by Walter Lacarbonara, Balakumar Balachandran, Jun Ma, J. A. Tenreiro Machado, and Gabor Stepan, 117–26. Cham: Springer International Publishing, 2020. https://doi.org/10.1007/978-3-030-34713-0_12.

[8] Horvath, Hanna Zsofia, and Denes Takacs. 'Stability and Local Bifurcation Analyses of Two-Wheeled Trailers Considering the Nonlinear Coupling between Lateral and Vertical Motions'. *Nonlinear Dynamics* 107, no. 3 (February 2022): 2115–32. https://doi.org/10.1007/s11071-021-07120-9.

[9] Flores, Paulo, and Hamid M. Lankarani. *Contact Force Models for Multibody Dynamics*. Vol. 226. Solid Mechanics and Its Applications. Cham: Springer International Publishing, 2016. https://doi.org/10.1007/978-3-319-30897-5.

[10] Polach, Oldrich. 'A Fast Wheel-Rail Forces Calculation Computer Code'. *Vehicle System Dynamics*, 33:sup1 (1999): 728-739. https://doi.org/10.1080/00423114.1999.12063125.